DOI: 10.1002/chem.200500616

Hydrogen Bonding and Dynamic Behaviour in Crystals and Polymorphs of Dicarboxylic–Diamine Adducts: A Comparison between NMR Parameters and X-ray Diffraction Studies

Roberto Gobetto,*[a] Carlo Nervi,[a] Michele R. Chierotti,[a] Dario Braga,*[b] Lucia Maini,[b] Fabrizia Grepioni,[b] Robin K. Harris,[c] and Paul Hodgkinson[c]

Abstract: Fumaric, malonic, maleic, and hydromuconic ($HOOCCH_2(CH)_2CH_2COOH$) acids were used to prepare a series of hydrogen-bonded adducts or salts, depending on whether acid–base proton transfer takes place, with the dibase [N-($\mu CH_2CH_2)_3N$] in various stoichiometric ratios. The resulting compounds have been investigated by using the ^1H MAS, ^{15}N, and ^{13}C cross polarisation magic-angle spinning (CPMAS) methods and discussed in relation to X-ray diffraction studies to ascertain the nature of the O-H···O, N···H-O, and N^+-H···O^- hydrogen bonds between the various species. In addition, two polymorphic forms of the malonic compound and a hydrate in the maleic case were examined. We also present the correlations between the chemical shifts of the hydrogen-bonded protons and those from the proton transfer reaction (acid-to-base) with the heavy atom distances. The dynamic behaviour in the solid-state of the [N-($\mu CH_2CH_2)_3N$] adducts with fumaric 2:1, maleic 1:1 hydrate, and hydromuconic acids, and a malonate 2:1 polymorph adduct have been investigated by using variable-temperature ^1H spin–lattice relaxation times. A substantial agreement between the activation energies obtained from fitting the T_1 data and the results of potential energy barrier calculations demonstrates that the facile reorientation of the [N-($\mu CH_2CH_2)_3N$] molecule occurs in several of the adducts.

Keywords: hydrogen bonds · NMR spectroscopy · polymorphism · relaxation times · supramolecular chemistry

Introduction

The controlled preparation and characterisation of crystal polymorphs,[1–7] that is, of different crystal forms of the same substance, is one of the major issues of modern crystal engineering and solid-state chemistry.[8–14] The reason for this interest stems from the fact that such studies can give fundamental information about molecular recognition, crystal nucleation, crystallisation, and the relationship between solid phases.[15–18] A key aspect of the studies on polymorphism is the possibility of preparing crystal forms by means of nonsolution methods, such as the solvent-free mechanochemical cogrinding of solids.[19–22]

The acid–base adducts investigated in this paper have also been selected in view of the fact that the main supramolecular interaction that holds the building blocks together is the hydrogen bond, undoubtedly the interaction of choice in the majority of crystal engineering investigations with molecular components.[23–29] The nature and strength of hydrogen-bonding interactions are being investigated extensively due to the requirements of crystal engineering. In the field of supramolecular chemistry, which has become one of the central topics in chemistry for the design of molecular systems,[30–33] the hydrogen-bonding interactions are often preferred because they combine directionality and strength

[a] Prof. R. Gobetto, Dr. C. Nervi, Dr. M. R. Chierotti
Dipartimento di Chimica I.F.M.
Università di Torino
Via P. Giuria 7, 10125 Torino (Italy)
Fax: (+39) 011-670-7855
E-mail: roberto.gobetto@unito.it

[b] Prof. D. Braga, Dr. L. Maini, Prof. F. Grepioni
Dipartimento di Chimica G. Ciamician
Università di Bologna
Via F. Selmi 2, 40126 Bologna (Italy)
Fax: (+39) 051-209-9456
E-mail: dario.braga@unibo.it

[c] Prof. R. K. Harris, Dr. P. Hodgkinson
Department of Chemistry, University of Durham
South Road, Durham, DH1 3LE (UK)

Supporting information for this article is available on the WWW under http://www.chemeurj.org/ or from the authors.

with selectivity.[34] Numerous papers devoted to the self-organization of organic molecules into one-, two-, or three-dimensional hydrogen-bonded architectures have been published in recent years.[35–43]

Solid-state NMR provides reliable information concerning hydrogen bonding and polymorphism.[44] This is mainly due to its ability to observe the change in the chemical shift of the atoms (in particular hydrogen, carbon, and nitrogen) directly involved in the interaction. By performing more sophisticated experiments[45] it is possible to obtain structural information such as the X–H distance and the X-H-Y angle from ^{13}C and ^{15}N chemical shift tensors, hetero- and homonuclear dipolar interactions, and quadrupolar interactions, and so on.

McDermott and co-workers[46] have shown that the isotropic ^{13}C chemical shift of carbonyl carbon atoms increases with decreasing heavy atom distance, whereas the ^{13}C chemical shift tensor parameters provide a clear indication of the protonation state of the carboxylic group. For the ^{15}N isotropic chemical shift the protonation-induced shifts are of the order of 100 ppm towards lower frequencies for aromatic amines and of about 25 ppm towards higher frequencies for aliphatic amines.[47] Furthermore, Limbach and co-workers[48] analysed ^{15}N chemical shift tensors in terms of the valence bond order model for pyridine and carboxylic acid adducts and found a correlation with the hydrogen-bond geometry. Frey and Sternberg[49,50] have observed direct relationships between δ ^{1}H and hydrogen-bond strength, and between δ ^{1}H and X–H distance, respectively, for different classes of hydrogen-bonded compounds.

In a previous paper we have investigated the proton transfer reaction along a hydrogen bond between aliphatic dicarboxylic acids and the diamine base 1,4-diazabicyclo-[2.2.2]octane (DABCO), by means of ^{1}H, ^{13}C, and ^{15}N solid-state NMR spectroscopy.[51] We founded that the isotropic ^{13}C chemical shift moved to higher frequencies as it passes from the carboxylic acid to the carboxylate form. The ^{13}C chemical shift tensor analysis of the carboxylic group showed that δ_{22} is the most sensitive parameter, changing from 192 ± 6 for the deprotonated form to 162 ± 5 ppm for the protonated form. Similar results had already been observed by several authors.[52,53] Correlation between the $\delta^{1}H$ and the heteroatom separation supports this interpretation.[54,55] The analysis of the compounds previously studied has shown that intramolecular O-H···O and intermolecular N···H-O hydrogen bonds are strong interactions with proton chemical shifts of around 16 ± 1.5 ppm, and N–O and O–O bond lengths of around 2.55–2.60 Å, while intermolecular N^{+}-H···O^{-} interactions are weaker and are characterised by a $\delta^{1}H$ of about 12.3 ppm and by a N–O bond length of about 2.7 Å.

It was possible to detect the occurrence of proton transfer between salts and cocrystals of dabco–dicarboxylic acid systems by using the NMR parameters.

In order to deepen our understanding of this fundamental interaction and to learn how to control proton transfer in hydrogen-bond formation we performed systematic studies of crystalline materials that have O-H···O, N-H···O, and O-H···N interactions.[44,51]

In this paper we expand our investigation into the hydrogen-bonding interactions of O-H···O, O-H···N, and N^{+}-H···O^{-} observed in the crystalline acid–base adducts to cases involving unsaturated aliphatic acids. These were obtained by treating a series of dicarboxylic acids (malonic acid, maleic acid, fumaric acid, and hydromuconic acid) with the dabco dibase. We subsequently investigated intriguing cases of polymorphism, hydrate formation, and different acid–base ratios.

The malonate salt $[HN(\mu CH_2CH_2)_3NH]$-$[OOC(CH_2)COOH]_2$ can be obtained as two polymorphs by reacting the acid and dabco in a 2:1 ratio. The polymorph achieved will depend on whether the crystals are obtained by grinding together the reactants (**I**) or by slow crystallization from solution (**II**).[56] In this case the solid-state NMR technique is necessary to ascertain the degree of protonation of the organic base. In another experiment the anhydrous salt $[HN(\mu CH_2CH_2)_3N][OOC(HC{=}CH)COOH]$ has been obtained by reacting maleic acid and the dabco base in absolute ethanol in the presence of a large excess of base. The salt contains chains of hydrogen-bonded cations $[HN(\mu CH_2CH_2)_3N]^{+}$ and isolated $[OOC(HC{=}CH)COOH]^{-}$ anions, forming exclusively intramolecular hydrogen bonds. Upon exposure to air the anhydrous salt converts within a few hours into the hydrated pseudopolymorphic species $[HN(\mu CH_2CH_2)_3N][OOC(HC{=}CH)COOH]\cdot(H_2O)_{0.25}$, that contains N^{+}-H···O^{-} hydrogen bonds between the anion and cation. Preliminary reports have been published on structural studies of these latter two cases.[57]

We were unable to fully characterise the nature of the adducts by diffraction techniques because of the intrinsic difficulty in locating the hydrogen atoms with this method. However, we are now able to complement such solid-state observations with the results of a combined ^{1}H MAS, ^{13}C CPMAS, and ^{15}N CPMAS solid-state NMR study.

To investigate the dynamic behaviour of the adducts in the solid-state we also performed a detailed study of ^{1}H wideline relaxation times at various temperatures. The optimised motional parameters calculated from the experimental spin–lattice proton relaxation time (T_1) data were then compared with the activation energies obtained by potential energy surface (PES) calculations.

Results and Discussion

The ^{1}H, ^{13}C, and ^{15}N NMR data for all compounds discussed herein are given in Table 1.

The ^{1}H MAS spectra are characterised by the signal due to dabco (CH_2 groups) that falls in the range 3.7–4.7 ppm, and an olefinic =CH signal for the acid at 6.8–7.3 ppm. Hydrogen-bonded protons, that is, N^{+}-H···O^{-} intermolecular and O-H···O intramolecular, and O-H···O intermolecular, can be observed in the range 12.9–20.9 ppm, depending on the interaction strength (see, for example, the ^{1}H MAS spec-

Table 1. ^{1}H, ^{13}C, and ^{15}N NMR data for all compounds.

Compound	δ ^{1}H [ppm]	Note	δ ^{13}C [ppm]	δ ^{15}N [ppm]
dabco–malonate 1:2	18.1	O-H···O intra	178.1 COO^-	0.0 N^+-H···O^-
(**I**)	13.6	N^+-H···O^-	172.5 COOH	
	4.2	dabco and CH_2	44.6 dabco	
		acid	38.4 CH_2	
dabco–malonate 1:2	17.8	O-H···O intra	174.4 COO^-	5.0 N^+-H···O^-
(**II**)		and N^+-H···O^-	173.2 COO^-	
	12.5	O-H···O inter	171.5 COOH	
		and N^+-H···O^-	44.7 dabco	
	3.6	dabco and CH_2	44.1 dabco	
		acid	37.4 CH_2	
dabco–maleate 1:1			169.6 COO^-	
anhydrous			137.9 CH	
(**III**)			47.6 dabco	
dabco–maleate 1:1	20.9	O-H···O intra	172.4 COO^-	3.8 N^+-H···O^-
hydrate	12.9	N^+-H···O^-	170.5 anhydrous	-17.3 free N
(**IV**)	7.3	CH	167.8 COOH	
	4.7	dabco	137.6 anhydrous	
			136.9 CH	
			46.1 anhydrous	
			44.1 dabco	
dabco–maleate 1:2	19.4	O-H···O intra	172.9 COO^-	6.3 N^+-H···O^-
(**V**)	14.9	N^+-H···O^-	167.8 COOH	
	7.0	CH	137.7 CH	
	4.3	dabco	135.3 CH	
			44.8 dabco	
dabco–fumarate 1:1	17.1	N^+-H···O^-	171.6 COO^-	
(**VI**)	16.7 (sh)	N^+-H···O^-	141.2 CH	
	7.1	CH	132.0 CH	
	3.8	dabco	44.6 dabco	
dabco–fumarate 1:2	15.7	N^+-H···O^- and	173.4 COO^-	5.3 N^+-H···O^-
(**VII**)		O-H···O inter	168.8 COOH	
	7.1	CH	137.8 CH	
	4.4	dabco	133.3 CH	
			44.6 dabco	
dabco–	18.5 (sh)	N^+-H···O^-	182.4 COO^-	1.9 N^+-H···O^-
hydromuconate 1:1	17.8	N^+-H···O^-	181.7 COO^-	
(**VIII**)	6.8 (sh)	CH	133.8 CH	
	3.7	dabco and CH_2 acid	133.0 CH	
			48.7 dabco	
			42.4 CH_2	

trum of dabco–maleate 1:2 (**V**) in Figure 1). The assignments for these spectra are based on previously published criteria.[51] The ^{13}C CPMAS spectra for these compounds (Figure 2 shows that of dabco–malonate 1:2, **I**) are similar to those previously reported for the dabco–dicarboxylic aliphatic acid adducts, although small differences can be observed. In particular the presence of the double bond shifts the carboxylic and carboxylate signals to about 167 and 173 ppm, respectively, whereas values of 177 (COOH) and 180 ppm (COO^-) have been observed in the dabco–aliphatic dicarboxylic acids.[44] It is straightforward to distinguish between the protonated and deprotonated forms on the basis of the relative chemical shift without performing a detailed tensor analysis on the carboxylic/carboxylate spectra.[58,59] The signals due to the =CH double bond appear around 137 ppm while the dabco signal is located at about 45 ppm.

Since it is well known that the nitrogen chemical shift caused by a hydrogen bond depends on many parameters including the heavy atom distance, the strength of the interaction and the hydrogen atom position along the axis of the heavy atoms, we also performed a systematic ^{15}N NMR study. As a general criterion, based on the previously published results,[51] the signals at around −15 ppm are assigned to nitrogen atoms not involved in the hydrogen bond, the resonances in the range −2 to −8 ppm

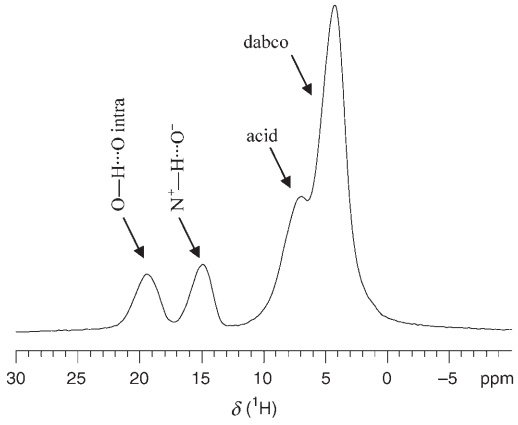

Figure 1. ^{1}H MAS NMR spectrum of dabco–maleate 1:2 (**V**) at 298 K obtained at 499.7 MHz.

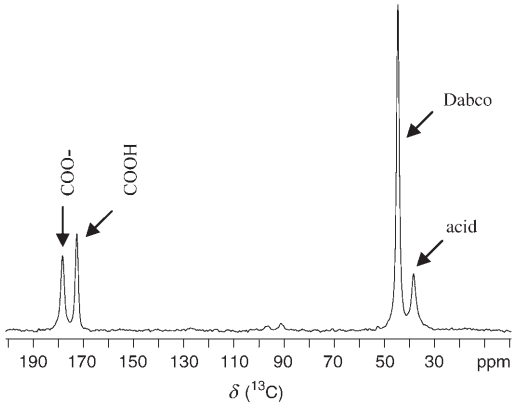

Figure 2. ^{13}C CPMAS NMR spectrum of dabco–malonate 1:2 (**I**) at 298 K obtained at 67.8 MHz.

are related to N···H-O interactions while a high-frequency shift to about 3–6 ppm indicates the presence of N^+-H···O^- interactions. Figure 3 shows the ^{15}N CPMAS spectrum of dabco–maleate 1:1 hydrate (**IV**) as an example of the free nitrogen signal and the N^+-H···O^- signal.

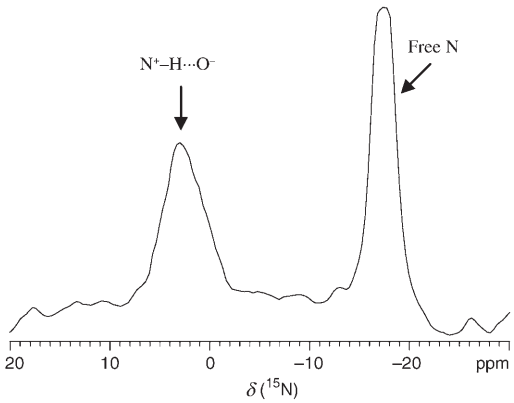

Figure 3. ^{15}N CPMAS NMR spectrum of dabco–maleate 1:1 hydrate (**IV**) at 298 K obtained at 27.25 MHz.

Dabco–malonate 1:2 (compounds I and II): The dabco–malonate 1:2 adduct, compound **I**, represents an intriguing case where the dabco ligand is diprotonated. The hydrogen malonate anion forms the typical intramolecular hydrogen bond with an O···O distance of 2.403(1) Å and interacts with the dabco moieties through an N···O hydrogen bond (length 2.713(1) Å) forming a supramolecular hydrogen-bonded adduct with the dabco units linked between two hydrogen malonate anions (Figure 4). The crystallographic asymmetric unit contains one independent hydrogen malonate anion and half a dabco unit. The presence of a carboxylate group

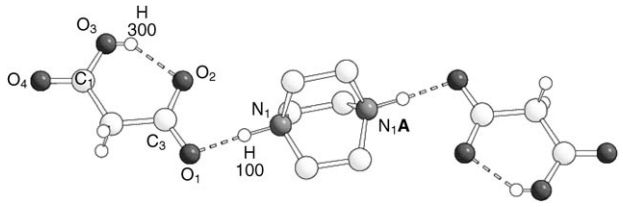

Figure 4. Crystal structure of dabco–malonate 1:2 (**I**). H_{CH} of dabco have been omitted for clarity.

in the acid is indicated by the nearly equal C–O distances [C3–O1 1.239(6) Å and C3–O2 1.253(7) Å] and by the peak at 178.1 ppm in the ^{13}C CPMAS spectrum (Figure 2), typical of a COO^- form. Nevertheless the ^{15}N resonance at 0.0 ppm for the two equivalent nitrogen atoms is intermediate between the chemical shift of a N^+–H-type and a weaker N···H form. This evidence confirms that the protonation of the two nitrogen atoms of dabco is not a straightforward process.[60]

The signal at 13.6 ppm in the ^1H MAS NMR spectrum and the N–O distance of 2.765(1) Å in **I** indicate the formation of two weak charge-assisted N^+-H···O^- hydrogen bonds between the diprotonated $[HN(\mu CH_2CH_2)_3NH]^{2+}$ ion and two hydrogen malonate anions. The remaining carboxylic groups [C1–O3 1.288(7) and C1–O4 1.196(6) Å], with ^{13}C resonances at δ 172.5 ppm, form intramolecular O-H···O hydrogen bonds as already observed in similar adducts. The proton chemical shift (δ 18.1) and the O–O distance of 2.403(1) Å suggest that this interaction is much stronger and of shorter length than the charge-assisted ones.

Polymorph **II** consists of two trimolecular units of the kind $acid^{intra}$–dabco–$acid^{inter}$ units joined by two $acid^{inter}$ anions that form a twelve-membered ring (Figure 5). Only

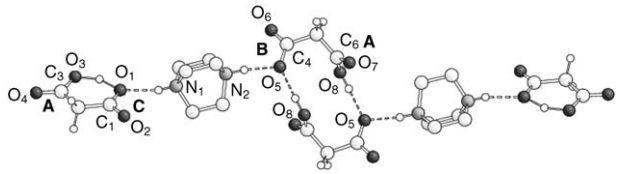

Figure 5. Crystal structure of dabco–malonate 1:2 (**II**). H_{CH} of dabco have been omitted for clarity.

three resonances are observed in the ^1H spectrum: δ 3.6, 12.5, and 17.8 ppm. The first is characteristic of the CH_2 groups present in the dabco and in the acid. The signal at 17.8 ppm is consistent with strong hydrogen bonds and we believe it corresponds to both the intramolecular hydrogen bond (O1···O3 2.429(2) Å) and to the shorter N2···O5 interaction [2.607(2) Å], while the signals of the intermolecular O5–O8 hydrogen bond [2.615(2) Å], and the longer N1···O1 [2.698(2) Å] both occur at 12.5 ppm. We partly resolved the potential ambiguity in the assignments for the hydrogen-bond signals by measuring the sample at 300 MHz. At this magnetic field, the signal at 17.8 ppm appears to broaden from 600 Hz linewidth (as seen at 500 MHz) to 700 Hz, while the signal at 12.5 ppm splits into a broadened 2:1 doublet, showing that at least the latter contains a component from a C–N carbon which involves a second-order effect arising from dipolar coupling to the quadrupolar ^{14}N nuclei.[61]

Although the two nitrogen atoms involved in the N^+-H···O^- (N1 and N2) interactions are slightly different, they give rise to a single resonance in the ^{15}N spectrum at 5.0 ppm which indicates the diprotonation of the dabco moiety. The ^{13}C spectrum of polymorph **II** shows three peaks in the carbonyl region at 174.4, 173.2 ppm, and a more intense resonance at 171.5 ppm. The resonance at 171.5 ppm is assigned to the carboxylic groups involved in the intramolecular O-H···O and the intermolecular O-H···O bonds labelled A in Figure 5, the C–O bond lengths of which are C3–O4 1.202(3), C3–O3 1.303(3), C6–O7 1.194(2), and C6–O8 1.314(2) Å. The chemical shifts of the remaining two signals (174.4 and 173.2 ppm) are characteristic of intermediate situations between carboxylic and car-

boxylate forms with different hydrogen-bond arrangements. This behaviour is intriguing, since the carboxylic acid carbon loses its proton in favour of the base but it still maintains a strong carboxylic character. This suggests a localisation of the negative charge on the oxygen atom involved in the intramolecular hydrogen bond and the N^+-H···O^- bond. The small differences in the C–O bond lengths [C4–O6 1.219(2), and C4–O5 1.275(2) Å labelled B, and C1–O2 1.219(2), and C1–O1 1.270(2) Å labelled C, in Figure 5] do not allow unambiguous assignment of the carboxylate peaks.

Dabco–maleate 1:1 (compounds III and IV): The remarkable feature of the anhydrous phase of dabco–maleate 1:1 (**III**) is the presence of N^+-H···N hydrogen-bonded dabco cation chains and isolated maleic anions (Figure 6). Due to its tendency to form the more-favoured cation–anion N^+-H···O^- interactions, compound **III** is very sensitive to air and also to grinding so it was not possible to run the ^{1}H MAS spectrum at the required high spinning rate without producing an extensive transformation of the sample. For the same reason several attempts to obtain ^{15}N data on this compound with long acquisition times failed. However, it was possible to record a ^{13}C spectrum that shows only one signal at 169.6 ppm in the carbonyl region for the two equivalent carboxylic groups, their chemical shift (169.6 ppm) being exactly between that of the COOH form (~167 ppm) and of the COO^- form (~173 ppm). This is also confirmed by crystallographic data: C1–O1 1.232(3), C1–O2 1.290(3), and C4–O4 1.225(3), C4–O3 1.285(4) Å. In the short intramolecular O-H···O [2.404(3) Å] bond, the hydrogen is situated almost midway along the bond and the single ^{13}C chemical shift is consistent with the presence of a symmetrical hydrogen bond.[62]

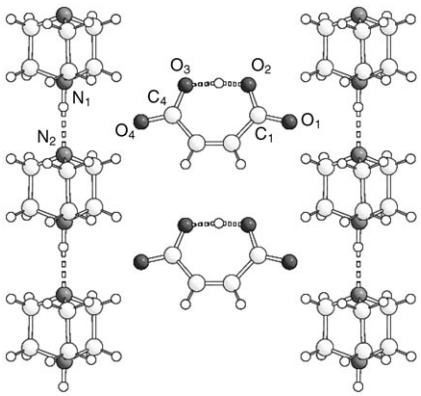

Figure 6. Crystal structure of dabco–maleate 1:1 anhydrous (**III**).

As previously described,[57] the anhydrous phase of dabco–maleate 1:1 (**III**) converts into dabco–maleate 1:1 hydrate $[HN(\mu CH_2CH_2)_3N][OOC(HC{=}CH)COOH]\cdot(H_2O)_{0.25}$ (**IV**) on simple exposure to air. During the conversion from anhydrous **III** to hydrated **IV** the N^+-H···N hydrogen bonds were replaced by more conventional "charge-assisted" N^+-H···O^- interactions which join together the acid and dabco units to form dimers. Concerning the crystal packing, a water molecule is also present that interacts with both the dabco and the acid through N···H-O [2.908(5) Å] and O···H-O [2.920(5) Å] vectors (Figure 7). The water molecule is located in a channel and is shared over two sites with occupancy 50:50. The water molecule signal is not observed separately in the ^{1}H spectrum probably because the signal is obscured by the aliphatic resonance of dabco ($\delta = 4.7$ ppm). In the new arrangement the delocalisation in the acid moiety is lost and it is possible to distinguish between a carboxylate [C4–O4 1.236(2), C4–O3 1.265(3), and C8–O8 1.237(2), C8–O7 1.255(3) Å], and a carboxylic group [C1–O1 1.221(3), C1–O2 1.287(3), and C5–O5 1.219(3), C5–O6 1.290(3) Å] as is confirmed by the presence of two resonances in the ^{13}C NMR spectrum at 172.4 (COO^-) and 167.8 ppm (COOH), respectively. The carboxylate groups are involved in the strong intramolecular O-H···O hydrogen bond [heavy atom separation of 2.417(3) and 2.427(3) Å corresponding to the signal at 20.9 ppm in the ^{1}H spectrum], and also in the relatively weak intermolecular N^+-H···O^- [2.688(3) and 2.728(3) Å] interactions, the ^{1}H signal of which falls at 12.9 ppm. We found two different types of nitrogen atoms in the dabco moiety that were characterised by ^{15}N peaks at 3.8 ppm (hydrogen bond acceptor in the intermolecular hydrogen bond) and −17.3 ppm (isolated nitrogen) (Figure 3).

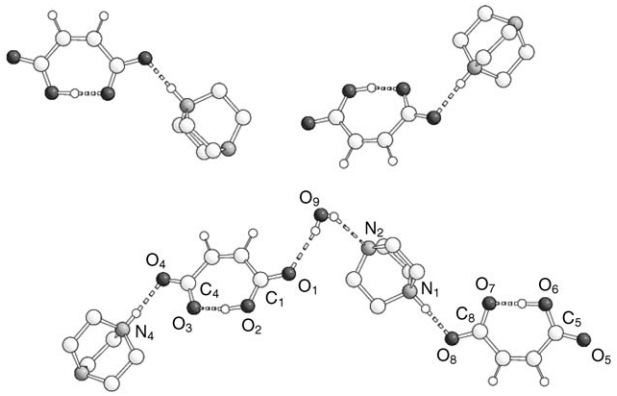

Figure 7. Crystal structure of dabco–maleate 1:1 hydrate (**IV**). H_{CH} of dabco have been omitted for clarity.

Dabco–maleate 1:2 (compound V): Crystals of $[HN(\mu CH_2CH_2)_3NH][OOC(HC{=}CH)COOH]_2$ (**V**), were obtained from a solution in ethanol, and the crystal structure determined. No significant differences were observed between our crystal structure and that previously published.[63] The latter has been used in this paper.

In compound **V** the dabco molecule forms a trimer with two acid molecules (Figure 8). The particular feature of **V** is that both acid moieties transfer their carboxylic proton to the nitrogen atoms of dabco, as confirmed by the single resonance at 6.3 ppm in the ^{15}N NMR spectrum. In this case, as

in all systems where the carboxylic acid is involved in more than one intramolecular hydrogen bond, the acid is able to transfer its hydrogen atom forming N^+-H···O^- interactions [2.662(3) and 2.614(4) Å, 14.9 ppm in the ^{1}H spectrum (Figure 1)]. The strong intramolecular O-H···O interactions [2.484(7) and 2.440(4) Å] are characterised by a ^{1}H resonance at 19.4 ppm. The ^{13}C spectrum of dabco–maleate 1:2 (**V**) shows two peaks in the carbonyl region at 172.9 ppm, assigned to the carboxylate groups [C7–O1 1.257(6), C7–O2 1.257(4) Å, and C11–O5 1.273(4), C11–O6 1.235(4) Å], and at 167.8 ppm that is related to the carboxylic groups [C10–O3 1.315(6), C10–O4 1.215(4), and C14–O7 1.319(4), C14–O8 1.212(4) Å].

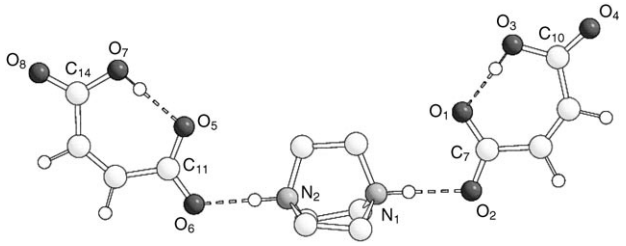

Figure 8. Crystal structure of dabco–maleate 1:2 (**V**). H_{CH} of dabco have been omitted for clarity.

Dabco–fumarate 1:1 (compound VI): Crystals of compound **VI** were obtained from a solution in ethanol and the crystal structure was determined at room temperature. Even though X-ray diffraction data at 150 K have been reported previously, we have chosen to discuss the results of the room-temperature NMR experiments on the basis of the former data for consistency.[64]

The adduct **VI** consists of an infinite chain of alternate acid and base units constructed around N···O interactions (Figure 9). As reported in the published results for compound **VI** one acidic hydrogen has been transferred completely from the acid to the base, while the other acidic hydrogen has been transferred only partially. In the former case, the hydrogen atom was located in two different sites in the Fourier map with occupancy 50:50. The C–O bond lengths [C4–O4 1.218(2), C4–O3 1.293(2), C1–O2 1.228(2), C1–O2 1.270(2)] show no clear distinction between the carboxylic and carboxylate group. This situation explains the ^{13}C spectrum where we see only one signal at 171.6 ppm in the appropriate region for the two types of carboxylic groups with a chemical shift in between those of a carboxylic and of a carboxylate group. The ^{1}H MAS spectrum is consistent with these data; in fact only one peak at 17.1 ppm with a shoulder at about 16.7 ppm is observed for the two N···O hydrogen bonds. Considering the N–O distances [N1–O3 2.577(1) and N2–O2 2.606(1) Å] the interactions can be classified as strong hydrogen bonds. It is worth noting that two strong intermolecular N^+-H···O^- interactions have not been found either in any of the other samples of this series or in the previously examined aliphatic dicarboxylic acid–dabco adducts.[44,51]

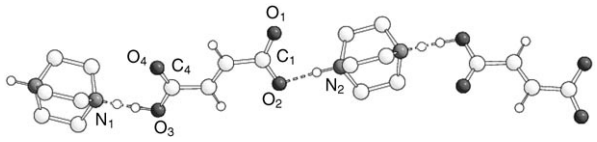

Figure 9. Crystal structure of dabco–fumarate 1:1 (**VI**). One acidic proton has been transferred only partially; the two different sites with occupancy 50:50 are shown. H_{CH} of dabco have been omitted for clarity.

In the ^{13}C spectrum the double-bond =CH resonances fall at 141.2 and at 132.0 ppm. Such a large difference is justified by the presence of a short intermolecular contact [C···H-C 2.854(1) Å, H···H 2.561(1) Å] between a C–H acid group and a CH_2 dabco moiety of the neighbouring chain, whereas the other acid C–H fragment is quite far from the neighbouring molecules, with C···H-C and H···H distances of 3.171(1) and 2.492(1) Å, respectively.[64] At room temperature the dabco unit gives rise to a very broad signal (700 Hz) centred at 44.6 ppm. This behaviour probably arises from the molecular motion having a similar timescale to the MAS rate, as described by Nakai and McDowell.[65] The dabco ^{13}C linewidth, recorded at 125 MHz, varied with temperature, being approximately 1400 Hz at −15 °C and about 400 Hz at −55 °C. Moreover, increasing the spin rate from 5 kHz to 7 kHz at room temperature sharpened the line from 700 Hz width to 500 Hz. Varying the decoupling power, on the other hand did not seem to change the width. Unfortunately the line-broadening associated with the same phenomenon precludes the observation of the ^{15}N resonance even at very long accumulation time.

Dabco–fumarate 1:2 (compound VII): As in the case of compound **VI** since the solid-state NMR measurements were carried out at room temperature, our crystal structure is used for discussion in preference to the one measured at 150 K although no significant differences were found.[64]

The crystal packing of adduct **VII** consists of acid chains based on intermolecular O-H···O hydrogen bonds linked by dabco molecules through N^+-H···O^- interactions (Figure 10). The ^{1}H MAS spectrum for compound **VII** shows only one resonance at 15.6 ppm for the two different O-H···O^- [2.540(3) Å] and N^+-H···O^- [2.644(2) Å] intermolecular hydrogen bonds. The resonance is very broad (approximately 3 ppm) indicating a partial overlapping of the two signals. The ^{13}C spectrum is characterised by two signals, one at 168.8 ppm for the COOH [C4–O3 1.195(3) and C4–O4 1.323(2) Å] involved in the intermolecular O-H···O^- bond between two acid molecules, and the other at 173.4 ppm, for the COO^- [C1–O1 1.239(3), C1–O2 1.268(3) Å]. The presence of a single resonance at 5.3 ppm in the ^{15}N spectrum confirms the diprotonation of the dabco moiety by carboxylic acids.

Dabco–hydromuconate 1:1 (compound VIII): The infinite chains formed by the A/B/A/B alternation of cations and anions observed in adduct **VI** is also present in compound

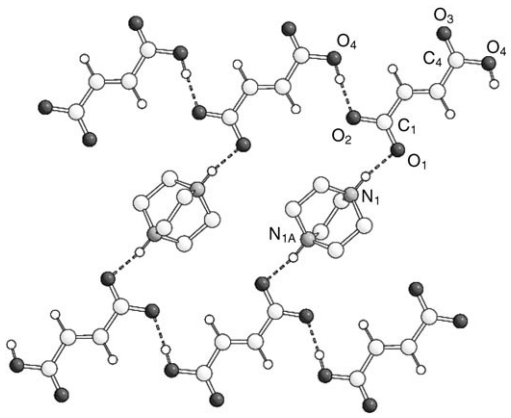

Figure 10. Crystal structure of dabco–fumarate 1:2 (**VII**). H_{CH} of dabco have been omitted for clarity.

VIII; the dabco unit is inserted into the original chains of acid molecules, but in this case no interchain linking is observed (Figure 11). The acid and dabco moieties are linked

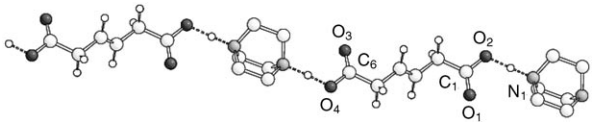

Figure 11. Crystal structure of dabco–hydromuconate 1:1 (**VIII**). H_{CH} of dabco have been omitted for clarity.

by N···O hydrogen-bond interactions. In both hydrogen bonds the hydrogen atom has been found close to the midpoint (see Table 2). The asymmetric unit contains one formula unit, that is, the two carboxyl groups are crystallographically independent as shown by the C–O bond lengths, namely, C1–O1 1.210(3) and C1–O2 1.280(3) Å, with a ^{13}C signal at 182.4 ppm, and C6–O4 1.303(3) Å and C6–O3 1.208(4) Å, with a ^{13}C signal at 181.7 ppm. The ^{13}C spectrum of compound **VIII** in the carbonyl region is similar to that of other aliphatic dicarboxylic adducts previously reported.[44] In the ^{1}H MAS spectrum of dabco–hydromuconate 1:1, one signal at 17.8 ppm with a shoulder at 18.5 ppm is present for the strong N^{+}-H···O^{-} interactions (N–O length: 2.555(3) and 2.577(4) Å). The ^{15}N spectrum of compound **VIII** is characterised by a broader, unresolved resonance centred at 1.9 ppm for the two semiprotonated nitrogen atoms involved in an N^{+}-H···O^{-} hydrogen bond.

Table 2. Bond lengths [Å] and angles [°] of the hydrogen-bond interactions in compound **VIII**.

Hydrogen bond	O–H	H–N	O···N	Angle
O2···H100···N1	1.35(5)	1.20(5)	2.555(4)	176(3)
O4···H400···N2	1.25(4)	1.33(4)	2.577(4)	175(3)

Proton relaxation studies and PES calculations: Spin-lattice proton relaxation times T_1 provide a versatile experimental route for evaluating molecular motion in the solid state. We decided to investigate the dynamic behaviour of the adducts by measuring the ^{1}H relaxation time at variable temperature in the wideline mode. Assuming that a single correlation time τ_c dominates the modulation of the dipolar interaction in the various temperature regimes, the T_1 values obey the Kubo–Tomita-type relation:[66]

$$T_1^{-1} = C[\tau_c/(1+\omega^2\tau_c^2) + 4\tau_c/(1 + 4\omega^2\tau_c^2)] \quad (1)$$

where C is the motional constant, ω is the angular Larmor frequency, and τ_c is the correlation time for the motion expressed by the Arrhenius law:

$$\tau_c = \tau_0 \exp(E_a/RT) \quad (2)$$

τ_0 and E_a are the correlation time in the limit of the infinite temperature and the activation energy for the motion, respectively.

Figure 12 reports the $\log T_1$ profile versus $10^3/T$ (K) for dabco–maleate 1:1 hydrate (**IV**). Similar profiles have also been obtained for dabco–malonate 1:2 (**II**), dabco–fumarate 1:2 (**VII**), and dabco–hydromuconate 1:1 (**VIII**) (see Experimental Section). The T_1 minimum is observed at about 310 K for hydrate **IV**, whereas for compound **VII** the T_1 minimum is found at about 350 K (see Supporting Information). For compounds **II** and **VIII** it was not possible to reach the T_1 minimum without decomposing the samples; nevertheless it was possible to obtain the E_a from the slopes of the lines used for fitting the points. Figure 12 shows the good agreement between the experimental data and the curves calculated according to the above Equations (1) and (2).

The best-fitted curves allow us to obtain the optimised motional parameters listed in Table 3. Thus for compound **IV** an E_a of 14.2 kJ mol^{-1} has been found, whereas for compounds **VII**, **II**, and **VIII** the activation energies are 21.3, 16.3, and 19.2 kJ mol^{-1}, respectively. The most likely dynamic process responsible for the T_1 profiles in the four adducts is the rotation of the dabco molecule around its C_3 symmetry axis. This has been confirmed by the semiempirical Austin Model 1 (AM1) PES calculations (Table 3, see Experimental Section for details) based on the structural data that provide possible models for the reorientational process. In fact, the relatively low energy barrier obtained from PES calculations (see Supporting Information) for compounds **II**, **IV**, **VII**, and **VIII**, indicates that dabco in these adducts should be able to rotate rather freely in the lattice at room temperature.

The experimental activation energies evaluated by fitting the T_1 values are in reasonable agreement with the calculat-

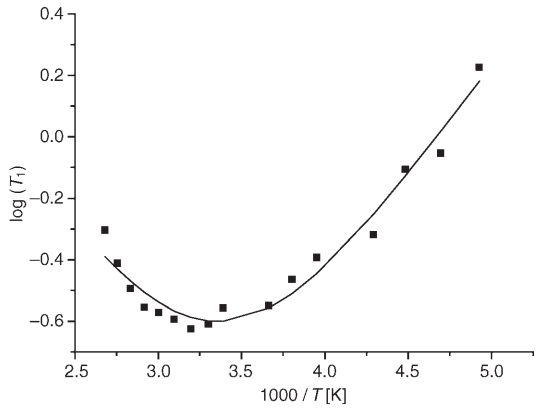

Figure 12. Variation of log of the spin-lattice relaxation time (T_1) with the temperature (1000/T) for the dabco–maleate 1:1 hydrate (**IV**).

Table 3. Calculations of the potential energy (PE) barriers associated with the rotation of the dabco for all adducts.

Compounds	Calculated dabco rotational barrier energies (H Opt, kJ mol^{-1})	Experimental dabco rotational barrier energies [kJ mol^{-1}]
malonic 2:1 (**I**)	42.53	–
malonic 2:1 (**II**)	39.12	16.3
maleic 1:1 (**III**)	69.34	–
maleic 1:1 hydrate (**IV**)	25.47	14.2
maleic 2:1 (**V**)	110.85	–
fumaric 1:1 (**VI**)	76.64	–
fumaric 2:1 (**VII**)	23.34	21.3
hydromuconic 1:1 (**VIII**)	21.63	19.2

ed PE barriers if one takes into account the crude approximation of the latter and a general overestimation of the potential barrier calculations within the "static environment" approximation. The activation energies obtained using PES and T_1 profiles for compounds **VII** and **VIII** differ by only approximately 2 kJ mol^{-1}. For compounds **IV** and **II** the discrepancy between calculated and experimental E_a values is slightly larger. In the barrier calculations rigid rotation is generally assumed, without considering the adaptability and the flexibility of the whole system. In the present study the mutual internal rigidity of the dabco unit and of the neighbouring molecules (an acceptable approximation in most of the cases) could lead, however, to an overestimation of the energy barriers. For compound **IV** the difference can be related to the presence of water molecules in the crystalline channel and to their mobility. In the PES calculations simultaneous motion of the dabco and the water molecules is not considered and so a higher E_a is expected. In contrast, the fumaric 1:1 and the anhydrous maleic 1:1 adducts, but in particular the maleic 2:1 adduct, appear to encounter very high potential energy (PE) barriers that freeze the dabco in its position (see Supporting Information). Moreover, the bottom of the PE well is rather narrow, surrounded by steeply rising potential walls, suggesting also that oscillation motion is limited. In all these cases the experimental values of the proton relaxation times (T_1 = 8.7, 20.3, 89.3 s for compounds **I**, **V**, and **VI**, respectively, at 295 K) are almost two orders of magnitude higher than in the case of fumaric 2:1, maleic 1:1 hydrate, and malonate 2:1 polymorph salts. In other words the lack of an efficient relaxation mechanism operating in the adducts experimentally confirms the substantial rigidity of the dabco moiety. For malonic 2:1 and malonic 2:1 polymorph an intermediate rotational energy barrier has been evaluated by PES calculations.

Conclusion

In this paper a complete solid-state characterisation of the adducts obtained from the reaction between dabco and dicarboxylic acids has been reported. By a combined use of X-ray diffraction and solid-state NMR data we demonstrated that in all adducts, except compound **VIII**, the N^+-H···O^- interactions are weak, with N–O bond lengths between 2.577 and 2.765 Å and ^{1}H chemical shifts in the range 12–15 ppm. Nevertheless, it is worth nothing that the simultaneous presence of two hydrogen bonds on the carboxylic group (either on the same oxygen or on two oxygen atoms) increases the proton acidity, favouring the proton transfer from the acid to the base. We can therefore tune the COOH acidity depending on the kind of hydrogen-bond network, allowing or disallowing the protonation or the diprotonation of dabco. We have also confirmed that all intramolecular O-H···O interactions are strong, with O–O lengths between 2.403 and 2.452 Å and ^{1}H chemical shifts ranging between 16.5 and 20.9 ppm. On the basis of the results reported here, the two main parameters for classifying the hydrogen bonds on the basis of their relative strengths are the proton chemical shift and the heavy atom separation. In weak hydrogen bonds, where the heavy atoms are separated by less than the sum of their van der Waals radii, that is, for O···H···O $\leq$ 2.6, N···H···N $\leq$ 2.8, and for N···H···O $\leq$ 2.7 Å, the proton chemical shifts appear at values smaller than 16 ppm. In strong hydrogen bonds the heavy atom separation is 2.4–2.55 Å for O···H···O, 2.6–2.7 Å for N···H···N and 2.5–2.6 Å for N···H···O, while the proton chemical shifts span 16–22 ppm. In Figure 13 the correlation between the hydrogen-bonded proton chemical shifts and the distance between heavy atoms is represented. The two lines, related to the N···H···O and the O···H···O interactions, show quite a different intercept value, but are rather similar in slope, agreeing with the correlations previously reported by several authors: in fact it is known that, independent of the nature of the heteroatoms involved, for strong hydrogen bonding the heavy atom separation is smaller, leading to an X–H bond polarization, which deshields the proton reso-

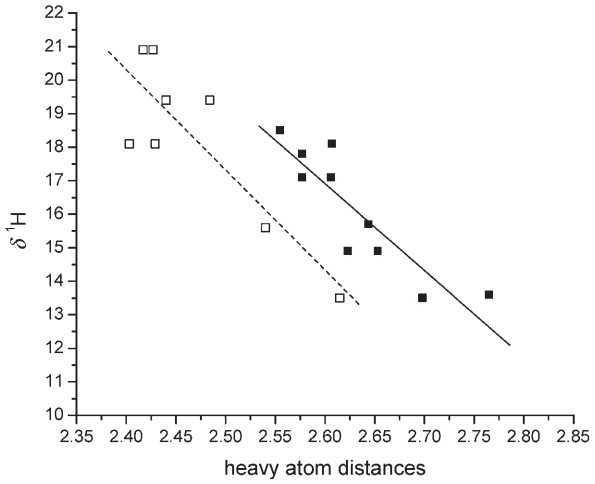

Figure 13. Correlation between ^{1}H chemical shifts [ppm] and heavy atom distances [Å] for the O···H···O interactions (□) and N···H···O interactions (■) for all compounds.

nance, while for weak hydrogen bonding the heavy atom separation is large so the X–H bond is less polarized and the proton resonance is less deshielded.[67]

Proton relaxation time measurements for compounds **II**, **IV**, **VII**, and **VIII** have indicated molecular motion in the adducts that acts as a mechanism of relaxation. Clearly the rotation of the dabco molecule is the source of this relaxation for the protons in the solid adducts. E_a values of 21.3, 14.2, 16.3, and 19.2 kJ mol^{-1} have been obtained for compounds **VII**, **IV**, **II**, and **VIII**, respectively, for the molecular motion. In general the experimental activation energies roughly agree with the potential barriers associated with the reorientation process on the basis of attractive and repulsive electrostatic interactions with atoms or nearby molecules. It is well known,[68] however, that potential barrier calculations within the "static environment" approximation tend to overestimate the barrier height.

In summary, while the NMR method affords quantitative information on the dynamic processes occurring in the solid state, the PE calculations based on the structural data provide possible models for the reorientation process.

Experimental Section

Solid-state NMR spectroscopy: ^{1}H MAS NMR spectra were recorded on a Varian Infinity Plus 500 spectrometer operating at 499.7 MHz for ^{1}H and on a Varian Unity Inova 300 spectrometer operating at 299.82 MHz for ^{1}H. Powdered samples were spun at about 25–28 kHz in a Varian 2.5 mm HX probe. Spectra were acquired using a $\pi/2$ pulse of 2.4 μs and a pulse delay of 20 s over a spectral width of 100 kHz. A total of four transients was collected for each spectrum. Proton chemical shifts were referenced through the resonance of poly(dimethylsiloxane) (PDMSO) at 0.14 ppm relative to TMS. All ^{13}C and ^{15}N spectra were recorded on a JEOL GSE 270 equipped with a Doty probe operating at 67.8 MHz for ^{13}C and 27.25 MHz for ^{15}N. A standard cross-polarisation pulse sequence has been used with a contact time of 3.5 ms for ^{13}C and 5 ms for ^{15}N, a 90° pulse of 4.5 μs, recycle delay of 10–15 s, and 600–4000 transients. Powdered samples were spun at 4–5 kHz at room temperature. The ^{13}C results were reported with respect to TMS assuming the hexamethylbenzene methyl peak is at 17.4 ppm. ^{15}N chemical shifts were referenced through the resonance of solid $(NH_4)_2SO_4$ (−355.8 ppm with respect to CH_3NO_2). For all samples the magic angle was carefully adjusted from the ^{79}Br spectrum of KBr by minimising the linewidth of the spinning sideband satellite transitions.

For the dabco–malonate 1:2 polymorph sample **II** ^{1}H MAS spectrum variable-temperature experiments were performed but no significant differences either in the linewidth, or in the chemical shifts were observed. Variable-temperature measurements were collected between 213 and 323 K by passing nitrogen gas through a heat exchanger immersed in liquid nitrogen.

***T*$_1$ measurements**: Proton spin-lattice relaxation times in wideline mode were measured by the inversion recovery pulse sequence on a JEOL GSE270 operating at 270.05 MHz for the proton. The 90° pulse duration was 1.0 μs. The temperature was maintained within ±2 K by a nitrogen gas flow (low temperatures) or air (high temperatures). The temperature was checked by a thermocouple set in the proximity of the sample (50 mg).

The error in the experimental E_a obtained by fitting the T_1 points with the Kubo–Tomita expression[66] has been estimated to be around ±1 kJ mol^{-1}.

Crystal structure determination: The crystal structure data for compounds **VI**, **VII** and **VIII** were collected at room temperature on a Nonius CAD4 diffractometer with $Mo_{K\alpha}$ radiation, $\lambda = 0.71073$ Å, and graphite monochromator. Crystal data and details of measurements are summarised in Table 4. SHELX97[69] was used for structure solution and refinement was based on F^2. Nonhydrogen atoms were refined anisotropically. H_N atoms were located in the final difference Fourier map and re-

Table 4. Crystal data and details of measurements.

	VI	**VII**	**VIII**
formula	$C_{10}H_{16}N_2O_4$	$C_{14}H_{20}N_2O_8$	$C_{12}H_{20}N_2O_4$
M_W	228.25	344.32	256.30
T [K]	293(2)	293(2)	293(2)
system	monoclinic	monoclinic	triclinic
space group	$P2_1/c$	$C2/c$	$P\bar{1}$
a [Å]	9.705(3)	20.027(6)	7.160(1)
b [Å]	8.939(3)	6.554(2)	7.722(7)
c [Å]	12.683(5)	12.516(5)	11.871(10)
α [°]	90	90	98.59(7)
β [°]	99.89(3)	114.87(3)	91.43(4)
γ [°]	90	90	96.08(4)
V [Å^3]	1083.9(7)	1490.5(9)	644.8(8)
Z	4	4	2
F(000)	488	728	276
ρ_{calcd} [Mg m^{-3}]	1.399	1.534	1.320
$\mu(Mo_{K\alpha})$ [mm^{-1}]	0.109	0.127	0.099
measured reflns	2859	1230	2376
unique reflns	2696	1162	2257
parameters	157	118	172
GOF on F^2	0.990	1.064	1.033
$R1$ (on F [$I > 2\sigma(I)$])	0.0479	0.0557	0.0697
$wR2$(on F^2, all data)	0.1533	0.1641	0.2090

fined without constraints. All other hydrogen atoms were added in calculated positions. SCHAKAL99 was used for the graphical representation. [70]

Powder diffractograms were measured for all species discussed in this paper and compared with those calculated on the basis of the single-crystal structure.

CCDC-271682–271684 contain the supplementary crystallographic data for this paper. These data can be obtained free of charge from The Cambridge Crystallographic Data Centre via www.ccdc.cam.ac.uk/data_request/cif/

Powder diffraction data were collected on a Philips PW-1710 automated diffractometer and on an X'Pert Philips diffractometer; both with $Cu_{K\alpha}$ radiation and graphite monochromator. The program PowderCell 2.2[71] was used for calculation of X-ray powder patterns.

Potential energy calculations: The calculations of the PE barriers associated with the rotation of the dabco unit around its N–N C_3 symmetry axis in the solid state were achieved by means of the AM1 semiempirical model,[72] as implemented in the Gaussian 03 program.[73] The structures used in the AM1 calculations were obtained from the corresponding cell packing by the inclusion of all the neighbouring molecules surrounding the dabco considered for the rotation. Typically between five and nine dabco units as well as between five and twelve acid moieties were selected for the calculations. This results in a large number (over 200) of atoms being included for the calculations, ruling out the possibility of using the ab initio methods. Therefore, the positions of hydrogen atoms were refined first by the universal force field (UFF) molecular mechanics method defining the atom types according to the experimental data, and in the second step by AM1. The structures obtained by this method were employed for the AM1 rigid PES calculations. We are aware of the fact that AM1 cannot accurately compute the position of hydrogen atoms directly involved in hydrogen bonds, and therefore the absolute value of energies in these calculations are of limited meaning. However these hydrogen atoms scarcely contribute to the definition of the PES barriers because of their axial position, and the energy barriers themselves were calculated as absolute differences between the minimum and the maximum energy values during PES.

Acknowledgements

We thank Dr. D. C. Apperley for assistance in the recording of some of the ^{1}H solid-state NMR spectra and for helpful discussions. We thank MIUR (PRIN and FIRB) and the Universities of Bologna and Torino for financial support. R.K.H. is grateful to the Leverhulme Trust for an Emeritus Fellowship.

[1] W. C. McCrone, *Polymorphism in Physics and Chemistry of the Organic Solid State* (Eds.: D. Fox, M. M. Labes, A. Weissenberger), Interscience, New York, **1965**.
[2] T. L. Threlfall, *Analyst* **1995**, *120*, 2435–2460.
[3] J. Bernstein, *Polymorphism in Molecular Crystals*, Oxford University Press, Oxford, **2002**.
[4] J. Bernstein, R. J. Davey, J. O. Henck, *Angew. Chem.* **1999**, *111*, 3646–3669; *Angew. Chem. Int. Ed.* **1999**, *38*, 3440–3461.
[5] J. D. Dunitz, J. Bernstein, *Acc. Chem. Res.* **1995**, *28*, 193–200.
[6] D. Braga, F. Grepioni, *Chem. Soc. Rev.* **2000**, *29*, 229–238.
[7] R. J. Davey, K. Allen, N. Blagden, W. I. Cross, H. F. Lieberman, M. J. Quayle, S. Righini, L. Seton, G. J. T. Tiddy, *CrystEngComm* **2002**, *4*, 257–264.
[8] D. Braga, G. R. Desiraju, J. S. Miller, A. G. Orpen, S. L. Price, *CrystEngComm* **2002**, *4*, 500–509.
[9] B. Moulton, M. J. Zaworotko, *Chem. Rev.* **2001**, *101*, 1629–1658.
[10] M. D. Hollingsworth, *Science* **2002**, *295*, 2410–2413.
[11] D. Braga, *Chem. Commun.* **2003**, 2751–2754.
[12] G. R. Desiraju, *Nature* **2001**, *412*, 397–400.
[13] L. Brammer, *Chem. Soc. Rev.* **2004**, *33*, 476–489.
[14] M. W. Hosseini, *CrystEngComm* **2004**, *6*, 318–322.
[15] N. Blagden, R. Davey, *Chem. Br.* **1999**, *35*, 44–47.
[16] N. Blagden, R. J. Davey, *Cryst. Growth Des.* **2003**, *3*, 873–885.
[17] R. K. R. Jetti, R. Boese, J. A. R. P. Sarma, L. S. Reddy, P. Vishweshwar, G. R. Desiraju, *Angew. Chem.* **2003**, *115*, 2008–2012; *Angew. Chem. Int. Ed.* **2003**, *42*, 1963–1967.
[18] P. Erk, H. Hengelsberg, M. F. Haddow, R. van Gelder, *CrystEngComm* **2004**, *6*, 474–483.
[19] N. Shan, F. Toda, W. Jones, *Chem. Commun.* **2002**, 2372–2373.
[20] A. V. Trask, N. Shan, W. D. S. Motherwell, W. Jones, S. H. Feng, R. B. H. Tan, K. J. Carpenter, *Chem. Commun.* **2005**, 880–882.
[21] A. V. Trask, W. D. S. Motherwell, W. Jones, *Chem. Commun.* **2004**, 890–891.
[22] D. Braga, F. Grepioni, *Angew. Chem.* **2004**, *116*, 4092–4102; *Angew. Chem. Int. Ed.* **2004**, *43*, 4002–4011.
[23] G. Gilli, P. Gilli, *J. Mol. Struct.* **2000**, *552*, 1–15.
[24] T. Steiner, *Angew. Chem.* **2002**, *114*, 50–80; *Angew. Chem. Int. Ed.* **2002**, *41*, 48–76.
[25] D. Braga, L. Maini, M. Polito, F. Grepioni, *Hydrogen Bonding Interactions Between Ions: A Powerful Tool in Molecular Crystal Engineering*, Springer, Berlin, **2004**, pp. 1–32.
[26] A. D. Burrows, *Struct. Bonding (Berlin)* **2004**, *108*, 55–95.
[27] P. Hubberstey, U. Suksangpanya, *Hydrogen-bonded Supramolecular Chain and Sheet Formation by Coordinated Guanidine Derivatives*, Springer, Berlin, **2004**, pp. 33–83.
[28] R. Vilar, *Hydrogen-bonding Templated Assemblies*, Springer, Berlin, **2004**, pp. 85–137.
[29] M. J. Hardie, *Hydrogen-bonded Network Structures Constructed from Molecular Hosts*, Springer, Berlin, **2004**, pp. 139–174.
[30] J. M. Lehn, *Supramolecular Chemistry: Concepts and Perspectives*, Wiley-VCH, Weinheim, **1995**.
[31] I. Haiduc, F. T. Edelmann, *Supramolecular Organometallic Chemistry*, Wiley-VCH, Weinheim, **1999**.
[32] J. W. Steed, J. L. Atwood, *Supramolecular Chemistry*, Wiley, New York, **2000**.
[33] G. R. Desiraju, *The Crystal as a Supramolecular Entity. Perspectives in Supramolecular Chemistry*, Wiley, Chichester (UK), **1996**.
[34] A. G. Jeffrey, W. Saenger, *Hydrogen Bonding in Biological Structures*, Springer, Berlin, **1991**.
[35] D. Braga, F. Grepioni, G. R. Desiraju, *Chem. Rev.* **1998**, *98*, 1375–1405.
[36] L. J. Prins, D. N. Reinhoudt, P. Timmerman, *Angew. Chem.* **2001**, *113*, 2446–2492; *Angew. Chem. Int. Ed.* **2001**, *40*, 2382–2426.
[37] L. Brammer, *Dalton Trans.* **2003**, 3145–3157.
[38] C. B. Aakeroy, K. R. Seddon, *Chem. Soc. Rev.* **1993**, *22*, 397–407.
[39] D. Braga, F. Grepioni, *Acc. Chem. Res.* **2000**, *33*, 601–608.
[40] A. M. Beatty, *CrystEngComm* **2001**, *3*, 243–255.
[41] K. Biradha, *CrystEngComm* **2003**, *5*, 374–384.
[42] H. W. Roesky, M. Andruh, *Coord. Chem. Rev.* **2003**, *236*, 91–119.
[43] A. M. Beatty, *Coord. Chem. Rev.* **2003**, *246*, 131–143.
[44] D. Braga, L. Maini, G. de Sanctis, K. Rubini, F. Grepioni, M. R. Chierotti, R. Gobetto, *Chem. Eur. J.* **2003**, *9*, 5538–5548.
[45] G. R. Goward, I. Schnell, S. P. Brown, H. W. Spiess, H. D. Kim, H. Ishida, *Magn. Reson. Chem.* **2001**, *39*, S5–S17.
[46] Z. T. Gu, R. Zambrano, A. McDermott, *J. Am. Chem. Soc.* **1994**, *116*, 6368–6372.
[47] G. C. Levy, R. L. Lichter, *Nitrogen-15 Nuclear Magnetic Resonance Spectroscopy*, Wiley, New York, **1979**.
[48] P. Lorente, I. G. Shenderovich, N. S. Golubev, G. S. Denisov, G. Buntkowsky, H. H. Limbach, *Magn. Reson. Chem.* **2001**, *39*, S18–S29.
[49] P. A. Frey, *Magn. Reson. Chem.* **2001**, *39*, S190–S198.
[50] U. Sternberg, E. Brunner, *J. Magn. Reson. Ser. A* **1994**, *108*, 142–150.
[51] R. Gobetto, C. Nervi, E. Valfrè, M. R. Chierotti, D. Braga, L. Maini, F. Grepioni, R. K. Harris, P. Y. Ghi, *Chem. Mater.* **2005**, *17*, 1457–1466.

[52] J. C. Williams, A. E. McDermott, *J. Phys. Chem.* **1993**, *97*, 12393–12398.
[53] L. Zheng, K. W. Fishbein, R. G. Griffin, J. Herzfeld, *J. Am. Chem. Soc.* **1993**, *115*, 6254–6261.
[54] A. McDermott, C. F. Ridenour, *Encyclopedia of NMR* (Eds.: D. M. Grant, R. K. Harris), Wiley, Chichester, **1996**, pp. 3820–3825.
[55] A. S. Mildvan, T. K. Harris, C. Abeygunawardana, *Methods Enzymol.* **1999**, 219–245.
[56] D. Braga, L. Maini, *Chem. Commun.* **2004**, 976–977.
[57] D. Braga, K. Rubini, L. Maini, *CrystEngComm* **2004**, *6*, 236–238.
[58] J. Herzfeld, A. E. Berger, *J. Chem. Phys.* **1980**, *73*, 6021–6030.
[59] M. M. Maricq, J. S. Waugh, *J. Chem. Phys.* **1979**, *70*, 3300.
[60] N. Someswara Rao, G. Babu Rao, B. N. Murthy, M. Maria Das, T. Prabhakar, M. Lalitha, *Spectrochim. Acta Part A* **2002**, *58*, 2737–2757.
[61] R. K. Harris, A. C. Olivieri, *Prog. Nucl. Magn. Reson. Spectrosc.* **1992**, *24*, 435–456.
[62] F. Fillaux, N. Leygue, J. Tomkinson, A. Cousson, W. Paulus, *Chem. Phys.* **1999**, *244*, 387–403.
[63] C. R. Sun, Z. M. Jin, *Acta Crystallogr. Sect. C* **2002**, *58*, O600–O601.
[64] K. F. Bowes, G. Ferguson, A. J. Lough, C. Glidewell, *Acta Crystallogr. Sect. B* **2003**, *59*, 100–117.
[65] T. Nakai, C. A. McDowell, *Chem. Phys. Lett.* **1994**, *227*, 639–644.
[66] R. Kubo, K. Tomita, *J. Phys. Soc. Jpn.* **1954**, *9*, 888–919.
[67] U. Sternberg, E. Brunner, *J. Magn. Reson. Ser. A* **1994**, *108*, 142–150.
[68] A. Gavezzotti, M. Simonetta, *Acta Crystallogr. Sect. A* **1976**, *32*, 997–1001.
[69] G. M. Sheldrick, SHELXL97, *Program for Crystal Structure Determination*, University of Göttingen (Germany), **1997**.
[70] E. Keller, SCHAKAL99, *Graphical Representation of Molecular Models*, University of Freiburg (Germany), **1999**.
[71] PowderCell, programmed by W. Kraus, G. Nolze, BAM, Berlin (Germany), subgroups were derived by Ulrich Müller (GH Kassel).
[72] M. J. S. Dewar, E. G. Zoebisch, E. F. Healy, J. J. P. Stewart, *J. Am. Chem. Soc.* **1985**, *107*, 3902–3909.
[73] Gaussian 98 (Revision A.9), M. J. Frisch, G. W. Trucks, H. B. Schlegel, G. E. Scuseria, M. A. Robb, J. R. Cheeseman, V. G. Zakrzewski, J. A. Montgomery Jr., R. E. Stratmann, J. C. Burant, S. Dapprich, J. M. Millam, A. D. Daniels, K. N. Kudin, M. C. Strain, O. Farkas, J. Tomasi, V. Barone, M. Cossi, R. Cammi, B. Mennucci, C. Pomelli, C. Adamo, S. Clifford, J. Ochterski, G. A. Petersson, P. Y. Ayala, Q. Cui, K. Morokuma, D. K. Malick, A. D. Rabuck, K. Raghavachari, J. B. Forestman, J. Cioslowski, J. V. Ortiz, A. G. Baboul, B. B. Stefanov, G. Liu, A. Liashenko, P. Piskorz, I. Komaromi, R. Gomperts, R. L. Martin, D. J. Fox, T. Keith, M. A. Al-Laham, C. Y. Peng, A. Nanayakkara, M. Challacombe, P. M. W. Gill, B. Johnson, W. Chen, M. W. Wong, J. L. Andres, C. Gonzales, M. Head-Gordon, E. S. Replogle, J. A. Pople, Gaussian Inc., Pittsburgh, PA, **1998**.

Received: May 31, 2005
Published online: November 3, 2005

